Eur. Phys. J. D (2020) 74: 63
https://doi.org/10.1140/epjd/e2020-100574-y

THE EUROPEAN PHYSICAL JOURNAL D

Regular Article

Third-order transport coefficient tensor of electron swarms in noble gases*

Ilija Simonović[1], Danko Bošnjaković[1], Zoran Lj. Petrović[2], Ronald D. White[3], and Saša Dujko[1,a]

[1] Institute of Physics, University of Belgrade, P.O. Box 68, 11080 Belgrade, Serbia
[2] Serbian Academy of Sciences and Arts, Knez Mihailova 35, 11001 Belgrade, Serbia
[3] College of Science and Engineering, James Cook University, 4810 Townsville, Australia

Received 14 November 2019 / Received in final form 11 February 2020
Published online 1 April 2020

Abstract. In this work we extend a multi term solution of the Boltzmann equation for electrons in neutral gases to consider the third-order transport coefficient tensor. Calculations of the third-order transport coefficients have been carried out for electrons in noble gases, including helium (He), neon (Ne), argon (Ar), krypton (Kr) and xenon (Xe) as a function of the reduced electric field, E/n_0 (where E is the electric field while n_0 is the gas number density). Three fundamental issues are considered: (i) the correlation between the longitudinal component of the third-order transport tensor and the longitudinal component of the diffusion tensor, (ii) the influence of the third-order transport coefficients on the spatial profile of electron swarm, and (iii) the errors associated with the two term approximation for calculating the third-order transport coefficients for electron swarms in noble gases. It is found that a very strong correlation exists between the longitudinal components of the third-order transport coefficient tensor and diffusion tensor for the higher values of E/n_0. The effects of the third-order transport coefficients on the spatial profile of electron swarms are the most pronounced for noble gases with the Ramsauer-Townsend minimum in the cross sections for elastic scattering. The largest errors of two term approximation are observed in the off-diagonal elements of the third-order transport coefficient tensor in Ar, Kr and Xe for the higher values of E/n_0.

1 Introduction

The investigation of charged particle transport in neutral gases has a wide range of applications, ranging from the modeling of swarm experiments [1–5] and modeling of low-temperature plasmas [6,7], to high-voltage technology [8] and modeling of particle detectors used in high-energy physics [9,10]. While there is a rich amount of data concerning the lower-order transport coefficients, including the drift velocity, diffusion coefficients and rate coefficients, for both electrons and ions, [11,12] and recently for positrons [13,14], the third-order transport coefficients are still largely unexplored as they are difficult to measure, and difficult to investigate theoretically.

The third-order transport coefficient tensor is required for the conversion of hydrodynamic transport coefficients into transport data that are measured in the arrival time spectra [15,16] and the steady-state Townsend experiments [4]. In addition, the third-order transport coefficients are needed for the representation of the spatial distribution of the swarm under conditions where this distribution deviates from the ideal Gaussian. Moreover, the third-order transport coefficients would be very useful in the swarm procedure for determining the sets of cross sections for the scattering of electrons and/or ions with neutral particles, if these transport coefficients were both calculated and measured with sufficient accuracy [17,18].

The third-order transport coefficients have been investigated by several authors. Whealton and Mason have determined the structure of the third-order transport tensor for an electric field only situation, and have calculated third-order transport coefficients for electrons assuming the constant collision frequency model gas [19]. Penetrante and Bardsley calculated the third-order transport coefficients for electrons in He, Ne and Ar by using the Monte Carlo simulations and a two term approximation for solving the Boltzmann equation [17]. Vrhovac and co-workers investigated the third-order transport tensor for electrons in He, Ne and Ar by employing the momentum transfer theory [18]. Koutselos studied the third-order transport coefficients of ions in atomic gases by using the molecular

* Contribution to the Topical Issue "Low-Energy Positron and Positronium Physics and Electron-Molecule Collisions and Swarms (POSMOL 2019)", edited by Michael Brunger, David Cassidy, Saša Dujko, Dragana Marić, Joan Marler, James Sullivan, Juraj Fedor.

[a] e-mail: sasa.dujko@ipb.ac.rs

dynamics simulations and a three-temperature method for solving Boltzmann's equation [21–24]. The equality of the higher-order transport coefficients between an electron swarm developing from multiple electron sources and another originating from a single electron source was investigated by Sugawara and Sakai [25]. The third-order transport coefficients for electrons in methane (CH_4) and sulfur hexafluoride (SF_6) have been recently investigated by Kawaguchi and co-workers via Monte Carlo simulations [16]. They have also derived the relation between the longitudinal third-order transport coefficient and the alpha-parameters, by using the theory of arrival time spectra of an electron swarm initially developed by Kondo and Tagashira [15]. Petrović and co-workers also recently investigated the third-order transport coefficient tensor for electrons in CH_4 by using Monte Carlo simulations and the multi term method for solving the Boltzmann equation [26]. Finally, Stokes and co-workers have studied the third-order transport coefficients for localized and delocalized charged-particle transport [27].

In this work we extend the multi term solution of Boltzmann's equation with the aim of investigating behavior of third-order transport coefficients in noble gases. As noble gases have simpler cross section sets than molecular gases, they are a good starting point for studying the third-order transport coefficients. Moreover, it is interesting to investigate the influence of the Ramsauer-Townsend minimum on the third-order transport tensor for electrons in Ar, Kr and Xe, as it can be expected that a rapid variation of the cross section for elastic collisions in these gases will leave a distinguishable signature on the profiles of the third-order transport coefficients. Moreover, if the components of the third-order transport tensor have very high values for electrons in Ar, Kr and Xe at low electric fields, due to the presence of the Ramsauer-Townsend minimum, they could also have a significant influence on the spatial profile of a swarm of electrons under these conditions.

The paper is organized as follows. In Section 2.1 we present the basic elements of the theory and definition of the third-order transport tensor. In Section 2.2 we describe the multi term method for solving the Boltzmann equation used in the present work where special emphasis is placed on the relating the third-order transport coefficients and the moments of the distribution function. In Section 3.1 we describe the cross sections used as an input to solve Boltzmann's equation and the conditions of our calculations. In Section 3.2 we analyze the E/n_0-dependence of mean energy for electrons in He, Ar, Kr and Xe. In Section 3.3 we investigate the variation of the third-order transport coefficients with E/n_0 for electrons in four noble gases. In Section 3.4 we study correlation between the longitudinal component of the third-order transport tensor and the longitudinal component of the diffusion tensor for electrons in He, Ne, Ar, Kr and Xe. In Section 3.5 we consider the influence of the third-order transport coefficients on the spatial profile of the swarm for electrons in these five gases. Finally, in Section 3.6 we discuss the errors associated with the two term approximation for solving the Boltzmann equation in the framework of calculations of the third-order transport coefficients for electrons in noble gases. Our conclusions are summarized in Section 4.

2 Theory: definitions and methods of calculation

2.1 Definition of the third-order transport coefficient tensor

In the present work, we consider a swarm of electrons which moves in an infinite and homogeneous background gas under the influence of a constant and uniform electric field. The z axis of the system is oriented along the direction of the electric field. The number density of electrons is very low and hence, the space charge effects and collisions between electrons are considered to be negligible. The background gas is regarded to be in a thermodynamic equilibrium at a temperature T_0, and the effect of the swarm on the state of the background gas can be neglected. The swarm of electrons is represented by the phase space distribution function $f(\mathbf{r}, \mathbf{c}, t)$, which is a function of position $\mathbf{r}$, velocity $\mathbf{c}$ and time t.

The continuity of the swarm in the configuration space is expressed by the following equation

$$\frac{\partial n(\mathbf{r},t)}{\partial t} + \nabla \cdot \mathbf{\Gamma}(\mathbf{r},t) = S(\mathbf{r},t), \tag{1}$$

where $n(\mathbf{r},t)$ is the number density of electrons, while $\mathbf{\Gamma}(\mathbf{r},t)$ and $S(\mathbf{r},t)$ are the flux of electrons and the source term, respectively. The number density of electrons can be expressed in terms of the phase space distribution function $f(\mathbf{r},\mathbf{c},t)$ as

$$n(\mathbf{r},t) = \int f(\mathbf{r},\mathbf{c},t)\,\mathrm{d}\mathbf{c}, \tag{2}$$

where integration is performed over the entire velocity space.

When the swarm is located far from boundaries of the system, and far from sources and sinks of charged particles, and when the applied electric field is spatially uniform, the swarm can enter the hydrodynamic regime [2,28]. In the hydrodynamic regime all space-time dependence of the phase space distribution function may be expressed in terms of functionals of the number density $n(\mathbf{r},t)$. Under the hydrodynamic conditions, the phase space distribution function can be represented by the following expression

$$f(\mathbf{r},\mathbf{c},t) = \sum_{k=0}^{\infty} \mathbf{f}^{(k)}(\mathbf{c},t) \odot (-\nabla)^k n(\mathbf{r},t), \tag{3}$$

where $\mathbf{f}^{(k)}(\mathbf{c},t)$ are time-dependent tensors of rank k and $\odot$ denotes a k-fold scalar product. This expression is known as the density gradient expansion of the phase space distribution function [28]. If the background electric field is static, the tensors $\mathbf{f}^{(k)}(\mathbf{c},t)$ are independent of time, after the swarm has relaxed to a stationary state. In the hydrodynamic regime, the flux of

velocity of charged particles is defined by the flux gradient relation

$$\mathbf{\Gamma}(\mathbf{r},t)=\sum_{k=0}^{\infty}\mathbf{\Gamma}^{(k+1)}\odot(-\nabla)^{k}\,n(\mathbf{r},t), \tag{4}$$

where the superscripts (k) denote the order of the density gradient, while $(k+1)$ denote the ranks of the tensors $\mathbf{\Gamma}^{(k+1)}$. These tensors represent the flux transport coefficients [29]. By truncating the flux gradient relation at $k=2$, the following equation is obtained

$$\begin{aligned}\mathbf{\Gamma}(\mathbf{r},t)=&\,\mathbf{W^{(f)}}n(\mathbf{r},t)-\mathbf{D^{(f)}}\odot\nabla n(\mathbf{r},t)\\&+\mathbf{Q^{(f)}}\odot(\nabla\otimes\nabla)\,n(\mathbf{r},t),\end{aligned} \tag{5}$$

where $\otimes$ is the tensor product, $\mathbf{W^{(f)}}$ and $\mathbf{D^{(f)}}$ are the flux drift velocity and the flux diffusion tensor, respectively, while $\mathbf{Q^{(f)}}$ defines the flux third-order transport coefficient tensor.

For an electric field only configuration, the third-order transport coefficient tensor has seven non-zero elements of which three are independent [19]. The independent components of the third-order transport tensor are $Q^{(f)}_{xxz}$, $Q^{(f)}_{zxx}$ and $Q^{(f)}_{zzz}$. Other non-zero components are related to the independent components by the following symmetry relations [19]:

$$Q^{(f)}_{xzx}=Q^{(f)}_{xxz}=Q^{(f)}_{yyz}=Q^{(f)}_{yzy}, \tag{6}$$

$$Q^{(f)}_{zyy}=Q^{(f)}_{zxx}. \tag{7}$$

The longitudinal and transverse third-order transport coefficients are defined as:

$$Q^{(f)}_{L}=Q^{(f)}_{zzz},\ Q^{(f)}_{T}=\frac{1}{3}(Q^{(f)}_{xxz}+Q^{(f)}_{xzx}+Q^{(f)}_{zxx}). \tag{8}$$

The hydrodynamic expansion of the source term is given by [28]

$$S(\mathbf{r},t)=\textstyle\sum_{k=0}^{\infty}\mathbf{S}^{(k)}\odot(-\nabla)^{k}\,n(\mathbf{r},t), \tag{9}$$

where the superscripts (k) denote the rank of tensors $S^{(k)}$ [29]. By substituting equations (5) and (9) into (1) the generalized diffusion equation, which is truncated at third-order gradients, is obtained. This equation can be written as

$$\begin{aligned}\frac{\partial n(\mathbf{r},t)}{\partial t}&+\mathbf{W}^{(b)}\odot\nabla n(\mathbf{r},t)-\mathbf{D}^{(b)}\odot(\nabla\otimes\nabla)\,n(\mathbf{r},t)\\&+\mathbf{Q}^{(b)}\odot(\nabla\otimes\nabla\otimes\nabla)\,n(\mathbf{r},t)=R_{\mathrm{prod}}n(\mathbf{r},t),\end{aligned} \tag{10}$$

where R_{prod} is the net particle production-rate, $\mathbf{W}^{(b)}$ and $\mathbf{D}^{(b)}$ are the bulk drift velocity and bulk diffusion tensor, respectively, and $\mathbf{Q}^{(b)}$ is the bulk third-order transport coefficient tensor. Bulk transport coefficients are related to the corresponding flux transport coefficients as [2,11,29]

$$\mathbf{W^{(b)}}=\mathbf{W^{(f)}}+\mathbf{S^{(1)}}, \tag{11}$$

$$\mathbf{D^{(b)}}=\mathbf{D^{(f)}}+\mathbf{S^{(2)}}, \tag{12}$$

$$\mathbf{Q^{(b)}}=\mathbf{Q^{(f)}}+\mathbf{S^{(3)}}. \tag{13}$$

Equation (10) cannot be solved analytically, even for the set of simple boundary conditions found in an idealized time-of-flight experiment [2]. However, this equation can be solved approximately if the Fourier transform of the solution is expanded in a Taylor series in terms of components of the third-order transport coefficient tensor [20]. The approximate solution up to the first-order can be written as [20]

$$\begin{aligned}n^{(1)}(\mathbf{r},t)=&\,n^{(0)}(\mathbf{r},t)\\&\times\left[1+Q_L^{(b)}\frac{t\left(z-W^{(b)}t\right)^3-6D_L^{(b)}t^2\left(z-W^{(b)}t\right)}{8\left(D_L^{(b)}t\right)^3}\right.\\&\left.+Q_T^{(b)}\frac{3t\left(z-W^{(b)}t\right)\left(x^2+y^2-4D_T^{(b)}t\right)}{8D_L^{(b)}t\left(D_T^{(b)}t\right)^2}\right],\end{aligned} \tag{14}$$

where $n^{(0)}(\mathbf{r},t)$ is the solution of the diffusion equation, which has the form [2]

$$n^{(0)}(\mathbf{r},t)=\frac{N_0e^{R_{\mathrm{prod}}t}e^{-\frac{\left(z-W^{(b)}t\right)^2}{4D_L^{(b)}t}-\frac{x^2+y^2}{4D_T^{(b)}t}}}{\left(4\pi D_T^{(b)}t\right)\sqrt{4\pi D_L^{(b)}t}}, \tag{15}$$

while N_0, $W^{(b)}$, $D_L^{(b)}$, $D_T^{(b)}$, $Q_L^{(b)}$ and $Q_T^{(b)}$ are the initial number of particles, bulk drift velocity, bulk longitudinal diffusion, bulk transverse diffusion, and bulk values of longitudinal and transverse third-order transport coefficients, respectively. Expression (14) has a simpler form in the relative coordinates that are defined as [20]

$$\chi_z=\frac{z-W^{(b)}t}{\sqrt{2D_L^{(b)}t}},\ \chi_x=\frac{x}{\sqrt{2D_T^{(b)}t}},\ \chi_y=\frac{y}{\sqrt{2D_T^{(b)}t}}. \tag{16}$$

In these coordinates the approximate solution (14) is given by

$$\begin{aligned}n^{(1)}(\mathbf{r},t)=&\,n^{(0)}(\mathbf{r},t)\\&\times\left(1+\frac{tQ_L^{(b)}}{\sigma_z^3}\chi_z(\chi_z^2-3)+\frac{3tQ_T^{(b)}}{\sigma_x^2\sigma_z}\chi_z(\chi_x^2+\chi_y^2-2)\right),\end{aligned} \tag{17}$$

where $\sigma_z=\sqrt{2D_L^{(b)}t}$ and $\sigma_x=\sigma_y=\sqrt{2D_T^{(b)}t}$. From this expression it can be seen that the contribution of the third-order transport coefficient tensor to the spatial profile of the swarm is proportional to $Q_L^{(b)}/(t^{1/2}(D_L^{(b)})^{3/2})$ and $Q_T^{(b)}/(t^{1/2}\sqrt{D_L^{(b)}}D_T^{(b)})$ [20].

2.2 Multi term solutions of Boltzmann's equation

The evolution of the phase space distribution function is given by the Boltzmann equation. In the case of a swarm of electrons, which are moving in an infinite and homogeneous background gas, the Boltzmann equation can be written as

$$\frac{\partial f}{\partial t}+\mathbf{c}\cdot\frac{\partial f}{\partial\mathbf{r}}+\frac{e}{m}(\mathbf{E}+\mathbf{c}\times\mathbf{B})\cdot\frac{\partial f}{\partial\mathbf{c}}=-J(f,f_0), \tag{18}$$

where e and m are the charge and mass of electrons, $\mathbf{E}$ and $\mathbf{B}$ are the electric and magnetic fields, and $J(f, f_0)$ is the collision operator. The Boltzmann equation is an integro-differential equation, which cannot be solved analytically in the case of electrons in real gases [2,6]. We employ the moment method where the phase space distribution function is expanded in terms of Burnett functions [28,30,31,33]:

$$\Phi_m^{[\nu l]}(\alpha\mathbf{c}) = N_{\nu l}\left(\frac{\alpha c}{\sqrt{2}}\right)^l S_{l+1/2}^{(\nu)}\left(\frac{\alpha^2 c^2}{2}\right) Y_m^{[l]}(\hat{\mathbf{c}}) = R_{\nu l}(\alpha c) Y_m^{[l]}(\hat{\mathbf{c}}), \tag{19}$$

where $Y_m^{[l]}$ is a spherical harmonic, while $S_{l+1/2}^{(\nu)}$ is a Sonine polynomial, α is a parameter and $\hat{\mathbf{c}}$ is a unit vector in velocity space [30,32]. The constant $N_{\nu l}$ is given by

$$N_{\nu l}^2 = \frac{2\pi^{3/2}\nu!}{\Gamma(\nu + l + 3/2)}, \tag{20}$$

where $\Gamma(\nu + l + 3/2)$ is the gamma function, while

$$R_{\nu l}(\alpha c) = N_{\nu l}\left(\frac{\alpha c}{\sqrt{2}}\right)^l S_{l+1/2}^{(\nu)}(\alpha^2 c^2/2), \tag{21}$$

determines the radial part of the Burnett function. The Burnett functions satisfy the orthogonality relations [30]:

$$\int \omega(\alpha, c)\Phi_m^{(\nu l)}(\alpha\mathbf{c})\Phi_{m'}^{[\nu' l']}(\alpha\mathbf{c})\mathrm{d}\mathbf{c} = \delta_{\nu'\nu}\delta_{l' l}\delta_{m' m}, \tag{22}$$

where

$$\omega(\alpha, c) = \left(\frac{\alpha^2}{2\pi}\right)^{3/2} e^{-\alpha^2 c^2/2}, \tag{23}$$

is the weighting function [30]. Orthogonality of the Burnett functions is due to orthogonality of the spherical harmonics and Sonine polynomials. The phase space distribution function can be expanded as

$$f(\mathbf{r}, \mathbf{c}, t) = \omega(\alpha, c)\sum_{\nu=0}^{\infty}\sum_{l=0}^{\infty}\sum_{m=-l}^{l} \mathbf{f}_m^{(\nu l)}(\alpha, \mathbf{r}, t)\Phi_m^{[\nu l]}(\alpha\mathbf{c}), \tag{24}$$

where $\mathbf{f}_m^{(\nu l)}(\alpha, \mathbf{r}, t)$ are the expansion coefficients which depend on the coordinates in the configuration space $\mathbf{r}$ and time t [30,32].

In the hydrodynamic regime the phase space distribution function can be expanded in terms of powers of the density gradient operator as [30,33–35]

$$f(\mathbf{r}, \mathbf{c}, t) = \omega(\alpha, c)\sum_{s=0}^{\infty}\sum_{\lambda=0}^{s}\sum_{\mu=-\lambda}^{\lambda}\sum_{\nu=0}^{\infty}\sum_{l=0}^{\infty}\sum_{m=-l}^{l} F(\nu l m|s\lambda\mu; \alpha, t)R_{\nu l}(\alpha, c)Y_m^{[l]}(\hat{\mathbf{c}})G_\mu^{(s\lambda)}n(\mathbf{r}, t), \tag{25}$$

where $F(\nu l m|s\lambda\mu; \alpha, t)$ are the moments of the phase space distribution function, while $G_\mu^{(s\lambda)}$ is the spherical form of the density gradient operator [30].

When the Boltzmann equation is multiplied by an arbitrary moment $F(\nu l m|s\lambda\mu; \alpha, t)$ and integrated over the entire velocity space, an infinite hierarchy of matrix equations in terms of moments $F(\nu l m|s\lambda\mu; \alpha, t)$ is obtained [31,33–35]. This hierarchy is truncated at a finite number of spherical harmonics $l = l_{\max}$, and a finite number of Sonine polynomials $\nu = \nu_{\max}$. The values of these numbers are determined by the criterion for convergence. The resulting system of equations is then solved numerically by using the matrix inversion. In our calculations, values of $l_{\max} = 4$ were sometimes required, when the phase space distribution function substantially deviates from an isotropy in the velocity space. Likewise, values of $\nu_{\max} = 80$ were required when the distribution function was far away from a thermal Maxwellian at the basis temperature T_b. The basis temperature is a parameter which is used to optimize the convergence.

The explicit expressions for determining the flux transport coefficients in terms of moments of the phase space distribution function can be obtained by expanding the flux of velocity of the charged particles $\mathbf{\Gamma}(\mathbf{r}, t)$ in terms of these moments and by recognizing terms which are contracted with the corresponding partial derivative of the number density $n(\mathbf{r}, t)$ [33–35]. The expansion of $\mathbf{\Gamma}(\mathbf{r}, t)$ in terms of $F(\nu l m|s\lambda\mu; \alpha, t)$ is given by

$$\Gamma_m^{[1]}(\mathbf{r}, t) = \int c_m^{[1]} f(\mathbf{r}, \mathbf{c}, t)\mathrm{d}\mathbf{c} = \int c_m^{[1]}\omega(\alpha, c)\sum_{s=0}^{\infty}\sum_{\lambda=0}^{s}\sum_{\mu=-\lambda}^{\lambda}\sum_{\nu=0}^{\infty}\sum_{l=0}^{\infty}\sum_{m'=-l}^{l} F(\nu l m'|s\lambda\mu; \alpha, t)R_{\nu l}(\alpha, c)Y_{m'}^{[l]}(\hat{\mathbf{c}})G_\mu^{(s\lambda)}n(\mathbf{r}, t)\mathrm{d}\mathbf{c}, \tag{26}$$

where $\Gamma_m^{[1]}(\mathbf{r}, t)$ is the flux of velocity of charged particles $\mathbf{\Gamma}(\mathbf{r}, t)$ written in the spherical form [30]. Cartesian components of a vector whose spherical form is given by

$$c_m^{(1)} = \sqrt{\frac{4\pi}{3}} c Y_m^{[1]}(\hat{\mathbf{c}}), \tag{27}$$

are given by the expressions [30]

$$c_x = \frac{i}{\sqrt{2}}\left(c_1^{[1]} - c_{-1}^{[1]}\right), \tag{28}$$

$$c_y = \frac{1}{\sqrt{2}}\left(c_1^{[1]} + c_{-1}^{[1]}\right), \tag{29}$$

$$c_z = -ic_0^{[1]}. \tag{30}$$

The components of the third-order transport coefficient tensor for an electric field only configuration are given by

$$Q_{xxz}^{(f)} = \frac{1}{\sqrt{2}\alpha}\Big(\mathrm{Im}\{F(011|221)\} - \mathrm{Im}\{F(01-1|221)\}\Big), \tag{31}$$

$$Q_{zxx}^{(f)} = -\frac{1}{\alpha}\left(\frac{1}{\sqrt{3}}\mathrm{Im}\{F(010|200)\} + \frac{1}{\sqrt{6}}\mathrm{Im}\{F(010|220)\}\right) + \frac{1}{\alpha}\mathrm{Im}\{F(010|222)\}, \tag{32}$$

and

$$Q^{(f)}_{zzz} = \frac{1}{\alpha}\left(\sqrt{\frac{2}{3}}\mathrm{Im}\{F(010|220)\} - \frac{1}{\sqrt{3}}\mathrm{Im}\{F(010|200\}\right), \tag{33}$$

where Re{} and Im{} refer to the real and imaginary parts of the moments $F(\nu lm|s\lambda\mu;\alpha,t)$, respectively [20]. The explicit expressions for the lower order transport coefficients in terms of moments of the phase space distribution function can be found in [33–35]. For brevity, in the following sections the superscript (f) in the flux third-order transport coefficients (and in the flux diffusion coefficients) will be omitted.

3 Results and discussion

3.1 Preliminaries

In this work we calculate the third-order transport coefficients for electrons in noble gases. Calculations are performed in the E/n_0 range between 10^{-4} Td and 100 Td (1 Td = 10^{-21} Vm^2). The temperature of the background gas T_0 is 293 K and thermal motion of background atoms is taken into account. All background atoms are assumed to be in the ground state. All electron scattering is considered to be isotropic. Elastic collisions are represented by the elastic momentum transfer cross section, while the inelastic collisions are represented by the total inelastic cross sections. For electrons in He we use the set of cross sections which has been detailed by Šašić *et al.* [36] while for electrons in Ne we use the set of cross sections, initially developed by Hayashi [37]. Likewise, for electron scattering in Ar and Xe we use the cross section sets developed by Hayashi [38,39]. For electrons in Kr we use the cross section set from a publicly available Monte Carlo code MAGBOLTZ [40].

3.2 Mean energy

In the following section we often find it necessary to refer to the mean energy of the electron swarm to understand and explain certain trends of the behavior of the third-order transport coefficients. Thus, in Figure 1 we show the mean energies of electrons in He, Ar, Kr and Xe as a function of E/n_0. Comparing the profiles of mean energy in He and the remaining three gases, we observe that the mean energy of electrons in He is different not only quantitatively, but also qualitatively. Specifically, there are four distinct regions of transport as E/n_0 increases for electrons in He and five distinct regions of transport in the case of Ar, Kr and Xe. First, for electrons in all considered gases, there is an initial plateau region where the mean energy is thermal. In the second distinct region of transport for electrons in He, the mean energy rises with an approximately constant slope in the log-log plot. The slope of mean energy is significantly lower in the third region, due to the influence of inelastic collisions. Finally, the slope is again increased in the fourth region. This

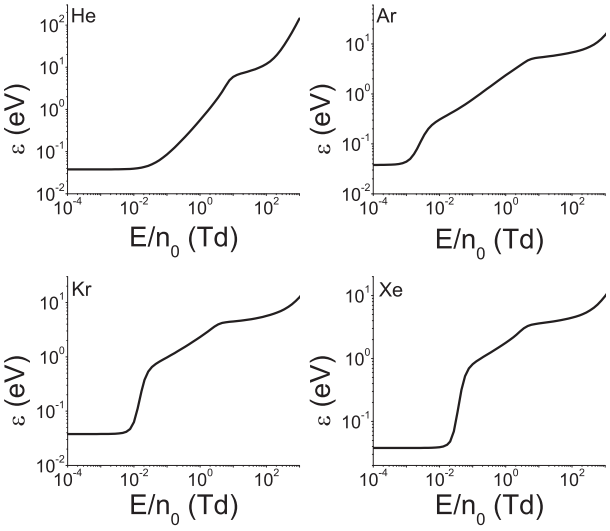

Fig. 1. Variation of the mean energy with E/n_0 for electron swarms in He, Ar, Kr and Xe.

increase can be attributed to a greater fraction of electrons being in the energy range where the collision frequency for all scattering processes reduces with increasing energy. For electrons in Ar, Kr and Xe, the rise of mean energy with increasing E/n_0 is very steep in the second distinct region of transport. A large fraction of electrons is thus in the energy range where elastic momentum transfer cross section is a monotonically decreasing function of energy, due to the presence of the Ramsauer-Townsend minimum. However, the slope of the mean energy is lower in the third region, in which high energy electrons are in the energy range where the elastic momentum transfer cross section is rising sharply. The slope of mean energy is further reduced in the fourth region where electrons can undergo inelastic collisions. Finally, this slope increases in the fifth distinct region of transport, in which the profile of mean energy changes from a power-law-like behavior to the more exponential-like increase. In this field region, the most energetic electrons are in the energy range where the collision frequency for all scattering processes is being reduced with increasing energy.

3.3 Variation of the third-order transport coefficients with E/n_0

3.3.1 Brief analysis

In Figure 2 we show the variation of the individual components of the third-order transport coefficient tensor with E/n_0 for electrons in He. We observe that $n_0^2 Q_{xxz}$ and $n_0^2 Q_{zzz}$ components are positive over the range of E/n_0 considered in the present work. However, the $n_0^2 Q_{zxx}$ component is negative until approximately 10 Td and positive at higher E/n_0. The absolute values of all individual components of the third-order transport tensor increase with increasing E/n_0 in the sub-excitation field region, which corresponds to the first two characteristic regions of the mean energy (see Fig. 1). This can be attributed

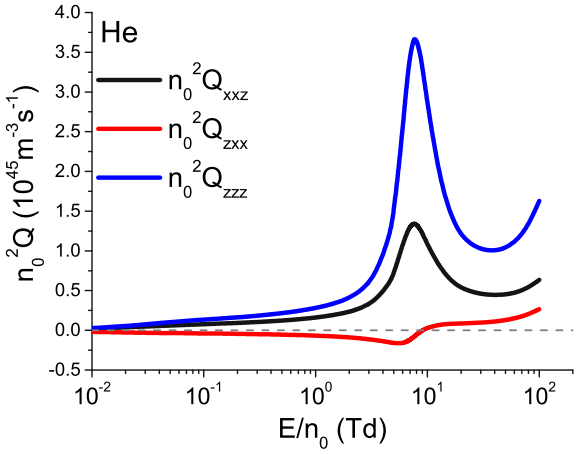

Fig. 2. Variation of $n_0^2Q_{xxz}$, $n_0^2Q_{zxx}$ and $n_0^2Q_{zzz}$ components of the third-order transport coefficient tensor with E/n_0 for electrons in He.

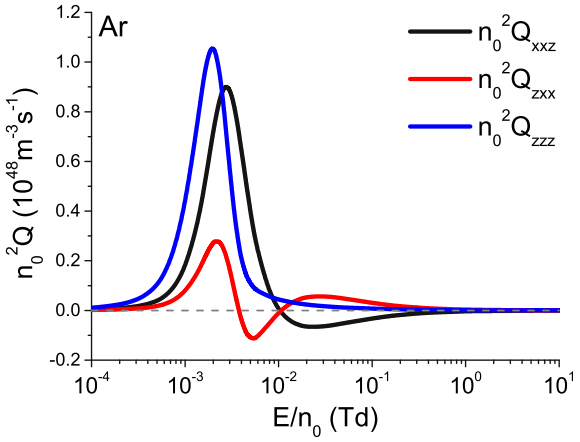

Fig. 3. Variation of $n_0^2Q_{xxz}$, $n_0^2Q_{zxx}$ and $n_0^2Q_{zzz}$ components of the third-order transport coefficient tensor with E/n_0 for electrons in Ar.

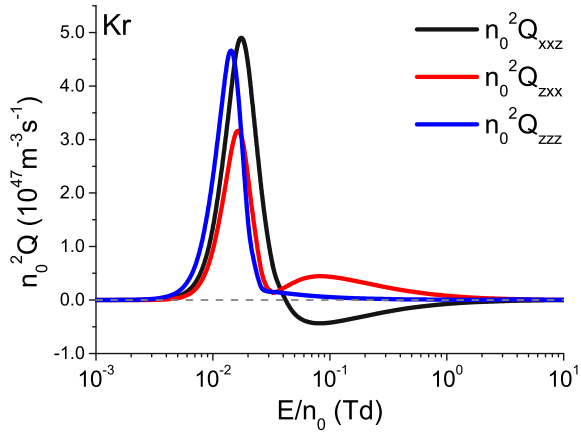

Fig. 4. Variation of $n_0^2Q_{xxz}$, $n_0^2Q_{zxx}$ and $n_0^2Q_{zzz}$ components of the third-order transport coefficient tensor with E/n_0 for electrons in Kr.

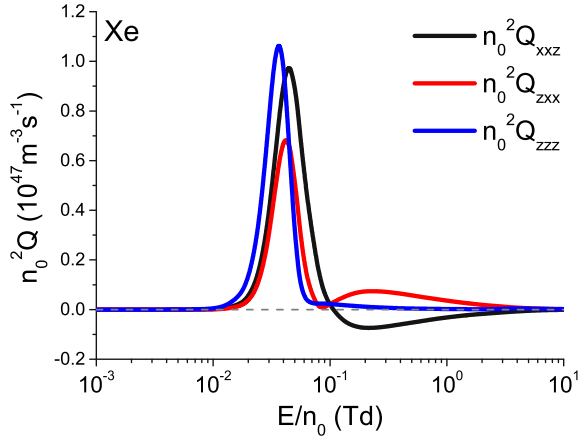

Fig. 5. Variation of $n_0^2Q_{xxz}$, $n_0^2Q_{zxx}$ and $n_0^2Q_{zzz}$ components of the third-order transport coefficient tensor with E/n_0 for electrons in Xe.

to a slow rise of elastic momentum transfer cross section in the energy range up to about 2 eV, as well as to its reduction at higher energies. However, the absolute values of all individual components of the third-order transport tensor are reduced for the higher values of E/n_0, where the high energy electrons can undergo many inelastic collisions. This field region roughly corresponds to the third characteristic region of the mean energy. Finally, all three components are increasing functions of E/n_0 in the limit of the highest fields considered in this work, where the collision frequency of the high energy electrons decreases with increasing electron energy.

In Figures 3–5 we show the variation of the individual components of the third-order transport coefficient tensor with E/n_0 for electrons in Ar, Kr and Xe, respectively. It can be seen that in these gases all components of the third-order transport tensor are rapidly rising functions of E/n_0 in the limit of the lowest fields, where most of the electrons are in the energy range in which the elastic momentum transfer cross section is reduced with the increase of energy, due to the presence of the Ramsauer-Townsend minimum. This field region corresponds to the first characteristic region of the mean energy, as well as to the first half of the second characteristic region of the mean energy, shown in Figure 1. However, all three components of the third-order transport tensor are rapidly decreasing functions of E/n_0 at higher fields, where the most energetic electrons are in the energy range in which the elastic momentum transfer cross section has a steep rise with an increase of energy. This field region corresponds to the second half of the second characteristic region of the mean energy. In the remaining field region considered in this work, $n_0^2Q_{zxx}$ and $n_0^2Q_{zzz}$ components exhibit a local minimum and a local maximum, while the $n_0^2Q_{xxz}$ component has a single local minimum only. The positions of these local maximums and local minimums correspond to those values of E/n_0 where the ratio between the mean energy and the position of the Ramsauer-Townsend minimum or the threshold of the first electronic excitation have similar values. For instance, the $n_0^2Q_{xxz}$ component becomes negative at the reduced electric field where the

mean energy is higher than the position of the Ramsauer-Townsend minimum by a factor that has values in the range between 1.3 and 1.4 for all three gases. Likewise, this component reaches the local minimum at approximately the same field where the $n_0^2 Q_{zxx}$ component reaches the second local maximum, and the mean energy is about 1.75 times higher than the energy of the Ramsauer-Townsend minimum at the position of these local extremes in all three gases. Moreover, the $n_0^2 Q_{zzz}$ component reaches the second local maximum at the value of the reduced electric field where the mean energy of electrons is about 2.5 times lower than the threshold of the first electronic excitation for all three gases (see Fig. 8). At the highest fields, where the most energetic electrons may undergo many inelastic collisions with the background atoms, the absolute values of all components of the third-order transport tensor are reduced with increasing E/n_0. This field region roughly corresponds to the fourth and the fifth characteristic regions of the mean energy in Ar, Kr and Xe. In the following subsubsection the E/n_0-profiles of the individual components of the third-order transport coefficient tensor for electrons in He, Ar, Kr and Xe are analyzed in a greater detail.

3.3.2 Comprehensive analysis

For electrons in He, the absolute values of all three components of the third-order transport tensor are monotonically increasing functions of E/n_0, but only in the limit of low electric fields. Specifically, $n_0^2 Q_{xxz}$ and $n_0^2 Q_{zzz}$ components rise in the field region below around 8 Td, where the mean energy of electrons is lower than 5 eV. Likewise, the absolute value of $n_0^2 Q_{zxx}$ increases up to approximately 5.9 Td, where the mean energy is around 3.6 eV. In the field region, where the absolute values of all three components are being increased with increasing E/n_0 most of the electrons undergo elastic collisions only. Moreover, the elastic momentum transfer cross section is gradually rising in the energy range between approximately 10^{-2} eV and 2 eV, while it is being reduced at higher energies. For this reason, resistance to diffusive motion that is caused by collisions of electrons with the background atoms is not very intensive in the field region up to approximately 5.9 Td. This in turn induces an increase of the absolute values of all three components of the third-order transport coefficient tensor in this range of E/n_0. However, at higher fields the most energetic electrons can undergo inelastic collisions with the background atoms, as the threshold for the first electronic excitation in helium is around 19.82 eV. This leads to a rapid decrease of $n_0^2 Q_{xxz}$ and $n_0^2 Q_{zzz}$ components in the field range between approximately 8 Td and 40 Td. Likewise, the increased resistance to the spreading of the swarm due to inelastic collisions leads to a rapid decrease of the absolute value of the $n_0^2 Q_{zxx}$ component in the field range between approximately 5.9 Td and 8 Td, and to a gradual increase of this component up to around 40 Td. For the higher values of E/n_0, all three components of the third-order transport coefficient tensor rise with increasing E/n_0. Over this range of E/n_0, the collision frequency of the most energetic electrons decreases with increasing E/n_0 which in turn enhances the third-order transport coefficients.

For electrons in Ar, Kr and Xe, all components of the third-order transport tensor are initially, rapidly increased with increasing E/n_0 for the lower values of E/n_0, as a large fraction of electrons is in the energy range where the elastic momentum transfer cross section markedly decreases with increasing energy, due to the presence of the Ramsauer-Townsend minimum in the cross sections for elastic scattering. These components reach local maximums in the E/n_0 region where the mean energy is lower than the position of the Ramsauer-Townsend minimum by a factor which is approximately between 2 and 3 in case of Ar, and approximately between 2 and 4 in case of Kr and Xe. Thus, all components of the third-order transport tensor start to decrease with an increase of E/n_0 in the E/n_0 region where the collision frequencies of the most energetic electrons increase with the rising energy of electrons.

The $n_0^2 Q_{zxx}$ component is the first to reach a local minimum in all three gases. However, the behavior of this component is somewhat different in the case of Ar, as compared to Kr and Xe. Specifically, this component becomes negative for electrons in Ar, while it remains positive over the entire considered range of E/n_0 for electrons in Kr and Xe. For electrons in Ar, the $n_0^2 Q_{zxx}$ component becomes negative at the value of E/n_0 where the mean energy is around 1.4 times lower than the position of the Ramsauer-Townsend minimum. The same component reaches a local minimum at the value of E/n_0 where the mean energy of the swarm is approximately equal to the energy position of the Ramsauer-Townsend minimum. However, in case of Kr and Xe this component reaches a local minimum at the value E/n_0 where the mean energy is around 1.25 times higher than the energy position of the Ramsauer-Townsend minimum. The $n_0^2 Q_{zxx}$ component becomes positive in Ar at approximately the same field, where the $n_0^2 Q_{xxz}$ component becomes negative. The $n_0^2 Q_{xxz}$ component starts to be negative at the value of E/n_0 where the mean energy is higher than the position of the Ramsauer-Townsend minimum by a factor of around 1.3 in case of Ar and Xe, and by a factor of approximately 1.4 in case of Kr. The sign of the $n_0^2 Q_{xxz}$ component remains unaltered until the end of the considered E/n_0 range for Ar, Kr and Xe. The $n_0^2 Q_{zxx}$ component reaches the second local maximum at approximately the same E/n_0 where the $n_0^2 Q_{xxz}$ component reaches the local minimum. The position of these local extremes for $n_0^2 Q_{xxz}$ and $n_0^2 Q_{zxx}$ components is at the value of E/n_0 where the mean energy is about 1.75 times higher than the position of the Ramsauer-Townsend minimum for electrons in all three gases. For the higher values of E/n_0, the absolute values of $n_0^2 Q_{xxz}$ and $n_0^2 Q_{zxx}$ are being reduced with increasing E/n_0 until the end of the considered field range.

The $n_0^2 Q_{zzz}$ component reaches a local minimum at the value of E/n_0 where the electrons with energies that are between approximately 2 and 3 times higher than mean energy, are in the energy range where the elastic momentum transfer cross section for electrons in Ar, Kr and Xe, is reduced (see Fig. 8) with increasing energy. For the higher E/n_0 values, the $n_0^2 Q_{zzz}$ component rises with

increasing E/n_0. This component reaches a local maximum at the value of E/n_0 where the electrons with energies that are about 2.5 times higher than the mean energy can undergo inelastic collisions with the background atoms. The absolute values of all three components of the third-order transport coefficient tensor are reduced with increasing E/n_0 at higher fields until reaching the end of the considered E/n_0 range.

At the qualitative level, the E/n_0-profiles of each component of the third-order transport coefficient tensor are very similar for electrons in Ar, Kr and Xe. Specifically, these components reach local maximums and local minimums at the values of E/n_0 at which the ratios between the mean energy and the position of the Ramsauer-Townsend minimum and/or the threshold for the first electronic excitation have very similar values. However, there is a significant difference in the profile of $n_0^2Q_{zxx}$ component for electrons in Ar, when compared to the corresponding profiles in Kr and Xe, as this component becomes negative in Ar. The absence of negative values of $n_0^2Q_{zxx}$ for electrons in Kr and Xe might be attributed to a steeper rise of the elastic momentum transfer cross section with an increasing energy, after the Ramsauer-Townsend minimum, in these two gases. As discussed recently by Simonović et al. [20] when the collision frequency is rising with increasing electron energy, one of the off-diagonal components of the third-order transport tensor ($n_0^2Q_{zxx}$ and $n_0^2Q_{xxz}$) is often negative. If the rise of the collision frequency with energy is not too steep, $n_0^2Q_{zxx}$ component is usually negative (and $n_0^2Q_{xxz}$ is positive). However, $n_0^2Q_{xxz}$ component is negative (and $n_0^2Q_{zxx}$ is positive) when the rise of the collision frequency with increasing electron energy is very steep.

3.4 Correlation between the longitudinal components of the skewness and diffusion tensors

Another issue that is highly relevant for understanding higher-order transport coefficients is the correlation between higher-order and lower-order transport coefficients. In this work we investigate the correlation between the longitudinal component of the third-order transport tensor and the longitudinal component of the diffusion tensor of electrons in noble gases. Recently, this correlation has been investigated for electrons in CH_4 [26]. It has been shown that whenever D_{zz} decreases, then Q_{zzz} is reduced markedly, and whenever D_{zz} increases in a decelerating way, Q_{zzz} also decreases, but less intensively. The Q_{zzz} was found to increase only when D_{zz} increases in an accelerating manner. It can be expected that this correlation is absent at the lowest E/n_0, as $n_0^2Q_{zzz}$ represents an asymmetric correction to diffusive motion and it vanishes in the limit of the lowest fields, unlike diffusion coefficients which have non-zero thermal values. For this reason $n_0^2Q_{zzz}$ is expected to rise with increasing E/n_0 at the lowest fields, regardless of the field dependence of n_0D_{zz}. The value of E/n_0 at which the correlation between the profiles of field dependence of $n_0^2Q_{zzz}$ and n_0D_{zz} occurs is different for various gases.

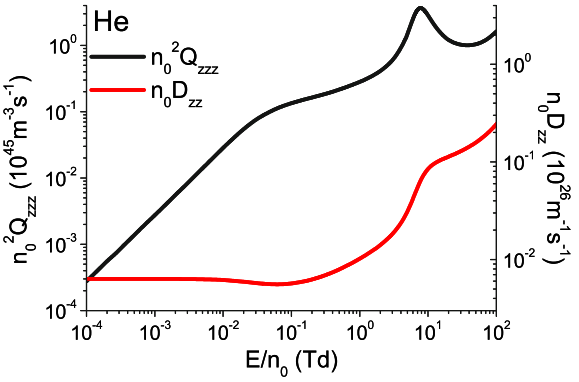

Fig. 6. The correlation of the longitudinal component of the third-order transport tensor $n_0^2Q_{zzz}$ and the longitudinal component of the diffusion tenzor n_0D_{zz} for electrons in He.

The correlation between the profiles of $n_0^2Q_{zzz}$ and n_0D_{zz} for electrons in He and Ne is shown in Figures 6 and 7, respectively. For electrons in He, $n_0^2Q_{zzz}$ and n_0D_{zz} rise with increasing E/n_0 in the E/n_0 region between approximately $5.9{\cdot}10^{-2}$ Td and 7.5 Td. This increase is the most intensive for E/n_0 between around 2.1 Td and 7.7 Td. However, between approximately 7.7 Td and 35 Td, the rise of n_0D_{zz} with increasing E/n_0 slows down, and n_0D_{zz} becomes a concave function of E/n_0 in the log-log plot. In this E/n_0 region, $n_0^2Q_{zzz}$ is reduced with increasing E/n_0. For E/n_0 between approximately 35 Td and 100 Td, the slope of n_0D_{zz} rises with E/n_0 and n_0D_{zz} becomes a convex function of E/n_0 in the log-log plot. As a consequence, in this E/n_0 region, $n_0^2Q_{zzz}$ rises monotonically with increasing E/n_0.

For electrons in Ne, $n_0^2Q_{zzz}$ and n_0D_{zz} decrease with increasing E/n_0 between approximately $3.5{\cdot}10^{-3}$ Td and $3.5{\cdot}10^{-2}$, and $n_0^2Q_{zzz}$ continues to decrease up to about $5.9{\cdot}10^{-2}$ Td. For the reduced electric fields higher than approximately $5.9{\cdot}10^{-2}$ Td, both $n_0^2Q_{zzz}$ and n_0D_{zz} rise with increasing field up to around 1.9 Td. This rise is especially rapid for E/n_0 between approximately 1 Td and 1.9 Td. At higher fields, n_0D_{zz} becomes a concave function of E/n_0 in the log-log plot, and it slowly decreases with increasing field for E/n_0 between approximately 5.9 Td and 30 Td, while it saturates at higher fields. In the E/n_0 region between approximately 1.9 Td and 100 Td, $n_0^2Q_{zzz}$ decreases monotonically with increasing E/n_0.

The correlation between the profiles of $n_0^2Q_{zzz}$ and n_0D_{zz} for electrons in Ar, Kr and Xe is shown in Figure 8. As can be seen, there is a very strong correlation between the profiles of $n_0^2Q_{zzz}$ and n_0D_{zz} for all three gases. It can also be seen that the profiles of $n_0^2Q_{zzz}$ and n_0D_{zz} in each of these gases are very similar. At the lowest E/n_0 $n_0^2Q_{zzz}$ and n_0D_{zz} rise with increasing E/n_0 in all three cases, as most of the electrons are in the energy range in which the elastic momentum transfer cross section decreases rapidly with increasing electron energy. The $n_0^2Q_{zzz}$ component reaches a local maximum at around $2.1{\cdot}10^{-3}$ Td, $1.4{\cdot}10^{-2}$ Td and $3.7\cdot10^{-2}$ Td for electrons in Ar, Kr, and Xe, respectively, while n_0D_{zz} reaches a local maximum at approximately $2.7{\cdot}10^{-3}$ Td, $1.7{\cdot}10^{-2}$ Td and $4.6{\cdot}10^{-2}$ Td,

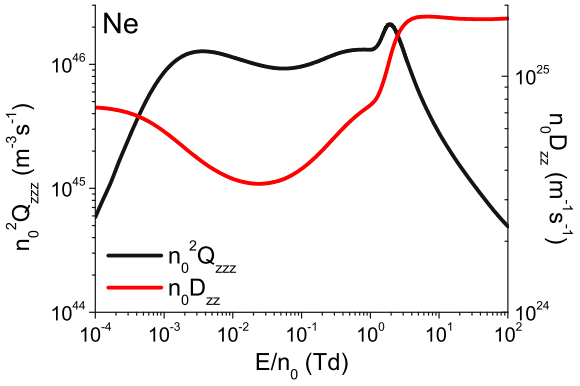

Fig. 7. The correlation of the longitudinal component of the third-order transport tensor $n_0^2Q_{zzz}$ and the longitudinal component of the diffusion tenzor n_0D_{zz} for electrons in Ne.

for electrons in Ar, Kr and Xe, respectively. In all three gases n_0D_{zz} reaches a local maximum at a somewhat higher E/n_0 as compared to $n_0^2Q_{zzz}$. After the local maximum, $n_0^2Q_{zzz}$ and n_0D_{zz} are decreased markedly with increasing E/n_0, up to around $5.9{\cdot}10^{-3}$ Td, $2.9{\cdot}10^{-2}$ Td and $7.7{\cdot}10^{-2}$ Td for electrons in Ar, Kr and Xe, respectively. For the higher values of E/n_0, these two quantities continue to decrease until reaching approximately 2.7 Td for electrons in Ar, and until reaching approximately 2.1 Td for electrons in Kr and Xe. However, the rate of decreasing of both $n_0^2Q_{zzz}$ and n_0D_{zz} is less intensive in this field region as compared to the lower fields. At higher fields, $n_0^2Q_{zzz}$ and n_0D_{zz} rise with increasing E/n_0 in a narrow field range. The $n_0^2Q_{zzz}$ component reaches the second local maximum at around 5.9 Td, 4.1 Td and 4.2 Td for electrons in Ar, Kr and Xe, respectively. After the second local maximum, the $n_0^2Q_{zzz}$ component decreases monotonically with increasing E/n_0 for the remaining E/n_0 in all three gases. In the field region around the second local maximum of $n_0^2Q_{zzz}$, the slope of n_0D_{zz} is significantly reduced with increasing E/n_0 up to about 13 Td for all three gases. At higher fields, n_0D_{zz} is saturated with increasing E/n_0.

In Figures 6–8 we observe a strong correlation between the profiles of $n_0^2Q_{zzz}$ and n_0D_{zz} for electrons in noble gases. Specifically, at relatively high enough fields $n_0^2Q_{zzz}$ decreases with increasing E/n_0 whenever n_0D_{zz} is a decreasing function of E/n_0, or when it increases as a concave function of E/n_0 in the log-log plot. The $n_0^2Q_{zzz}$ increases only at the lowest fields, and in those regions of E/n_0 where n_0D_{zz} raises with increasing field as a convex (or possibly linear) function in the log-log plot. The correlation between $n_0^2Q_{zzz}$ and n_0D_{zz} can be understood on an intuitive level. The third-order transport tensor represents an asymmetric deviation of the total diffusive motion, from the motion which is represented by the diffusion tensor. Thus, the third-order transport tensor describes a small correction to total diffusion. For this reason, the motion which is represented by the third-order transport tensor 'carries' a much smaller amount of energy and momentum than the motion which is described by the diffusion tensor. As a consequence, this transport

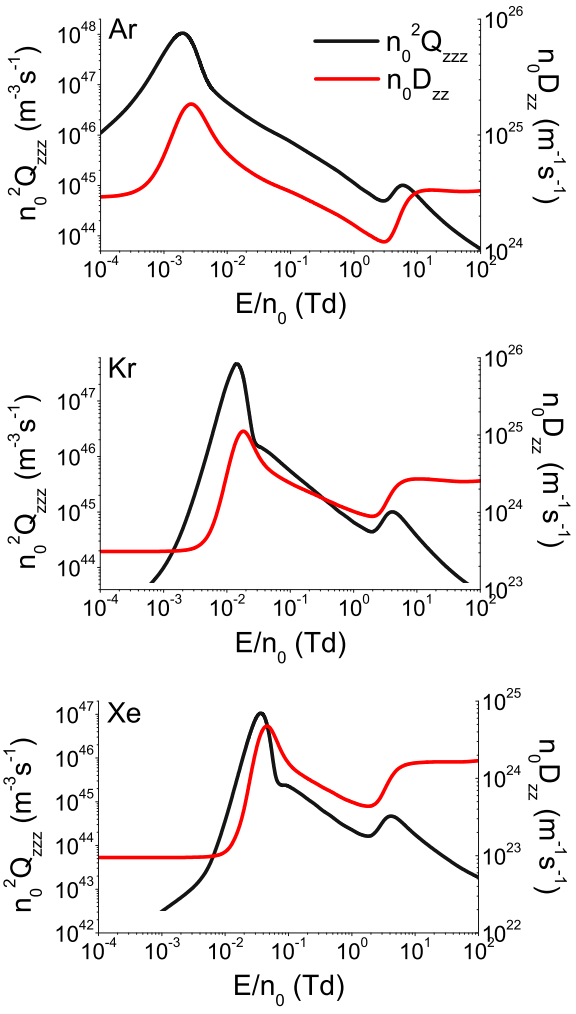

Fig. 8. The correlation of the longitudinal component of the third-order transport tensor $n_0^2Q_{zzz}$ and the longitudinal component of the diffusion tenzor n_0D_{zz} for electrons in Ar, Kr and Xe.

property is much more sensitive with respect to the collisions between the electrons and the background atoms. This leads to a reduction of the $n_0^2Q_{zzz}$ component with increasing E/n_0 (at high enough fields) whenever the resistance to diffusive motion due to collisions is intensive enough to cause a decrease of n_0D_{zz} or even a decelerated rise with increasing E/n_0. The correlation of the longitudinal component of the third-order transport tensor and the longitudinal component of the diffusion tensor is important for two reasons. Firstly, it enables an easier understanding of the E/n_0-dependence of the third-order transport coefficients in comparison to the direct analysis from the cross sections and from the variation of the mean energy with E/n_0, which might be sometimes difficult. Secondly, the correlation between $n_0^2Q_{zzz}$ and n_0D_{zz} shows that the third-order transport coefficients are more sensitive with respect to the energy dependence of the cross sections than the diffusion coefficients. This suggests that the third-order transport coefficients would be very useful in swarm procedure for determining and

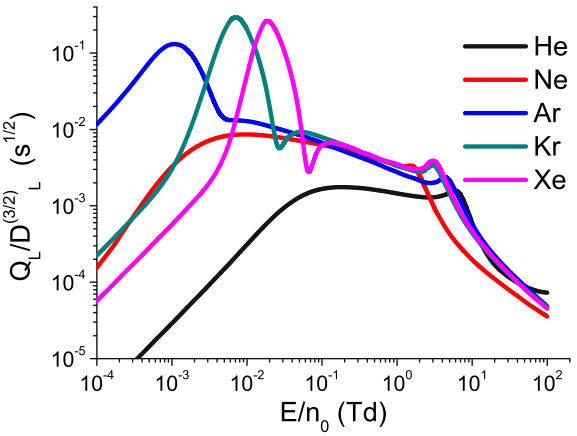

Fig. 9. The values of ratio $Q_L/(D_L)^{3/2}$ for electron swarms in He, Ne, Ar, Kr and Xe as functions of the reduced electric field E/n_0. Calculations have been performed assuming the gas number density of 3.54×10^{22} m^{-3}.

normalizing the cross section sets, if they were both calculated and measured with a sufficient accuracy.

3.5 Effects of the third-order transport coefficients on the spatial profile of the swarm

In this work, we also investigate the influence of the third-order transport coefficients on the spatial profiles of the swarm of electrons in noble gases. As was shown in [27], the components of the third-order transport tensor represent an asymmetric deviation of the spatial profile of the swarm of charged particles from an ideal Gaussian, which represents the solution of the diffusion equation. Specifically, the longitudinal component of the third-order transport tensor describes longitudinal elongation or compressing of the swarm along the longitudinal direction, while the off-diagonal components describe transverse elongation or compressing of the swarm along the longitudinal direction. It can be seen from equation (17) that the contribution of the third-order transport coefficients to the spatial profile of the swarm is proportional to $Q_L/(t^{1/2}(D_L)^{3/2})$ and $Q_T/(t^{1/2}\sqrt{D_L}D_T)$.

In Figure 9 we show the ratio $Q_L/(D_L)^{3/2}$ for electrons in noble gases as a function of E/n_0. It should be emphasized that in Figure 9 we show the ratio where the flux values of Q_L and D_L are assumed, although the influence of the third-order transport coefficients on the spatial profile of the swarm is proportional to the corresponding ratio of the bulk values of Q_L and D_L. The reason for this is a much better accuracy of our multi term results when compared to our Monte Carlo results, and our current inability to obtain the bulk values from our multi term code. However, the difference between the flux and the bulk values of the longitudinal components of the third-order transport coefficient tensor is within statistical uncertainty of Monte Carlo simulations up to about 21 Td in He and Ne, and up to 100 Td in Ar, Kr and Xe. Moreover, we are principally interested in the field dependence of this ratio for E/n_0 less than 10 Td, due to the presence of local maximums and local minimums in this particular field range. For this reason, we investigate the field dependence of the ratio $Q_L/(D_L)^{3/2}$ assuming the flux values of Q_L and D_L.

We may observe in Figure 9 that the ratio $Q_L/(D_L)^{3/2}$ increases monotonically with increasing E/n_0 in the limit of the lowest E/n_0 (below 10^{-3} Td). For the higher values of E/n_0 (higher than 10 Td) we see that this property decreases monotonically with increasing E/n_0 for electrons in all considered gases. At intermediate fields, however, this ratio reaches several local maximums and local minimums. Specifically, this ratio has only a single local maximum for electrons in Ne, at around 0.01 Td[1]. For electrons in He and Ar, this ratio has two local maximums and one local minimum. In the case of He these local maximums are at about 0.21 Td and 5.9 Td, and both of these maximums are of a similar magnitude. However, in the case of Ar, the first local maximum at around 10^{-3} Td is much higher than the other local maximum at about 4.6 Td. This difference is caused by the presence of the Ramsauer-Townsend minimum in the elastic cross section of Ar. The local minimum is shallow, and it is at around 2.7 Td in both gases. For electrons in Kr and Xe, the investigated ratio has three local maximums and two local minimums. The first local maximum occurs at about $7\cdot10^{-3}$ Td and $1.9\cdot10^{-2}$ Td for electrons in Kr and Xe, respectively, and is quite high in both gases, due to the presence of Ramsauer-Townsend minimum in the cross sections for elastic scattering. This maximum is followed by a local minimum at about $2.7\cdot10^{-2}$ Td for electrons in Kr and at around $6.8\cdot10^{-2}$ Td for electrons in Xe. The second local maximum of this ratio is at around 0.046 Td and 0.13 Td for electrons in Kr and Xe, respectively. The last local minimum is at about 2.1 Td, and it is quite shallow in both Kr and Xe. The third local maximum is at about 2.7 Td in both gases. In the case of electrons in Ar, Kr and Xe the value of E/n_0 at which $Q_L/(D_L)^{3/2}$ reaches the first local maximum is about 2 times lower than the value of E/n_0 where Q_L reaches the first local maximum. This is expected, on a qualitative level, as $Q_L/(D_L)^{3/2}$ reaches the first local maximum after D_L starts rising with increasing E/n_0, but before reaching the first peak.

The ratio $Q_L/(D_L)^{3/2}$ has the highest values for Ar, Kr and Xe near the position of the first local maximum. Thus, the contribution of the third-order transport coefficients to the spatial profile of the swarm is the most pronounced exactly for these conditions. However, it must be emphasized that the approximate expression (17) has been derived under an assumption that transport coefficients are constant in time, from the initial time ($t = 0$). As this condition is satisfied only after relaxation of the swarm to the stationary state, the expression (17) is not applicable to the early stages of swam development

[1] There is an additional local maximum of this ratio at around 1.5 Td for electrons in neon, that is preceded by a local minimum at around 1.2 Td. However, both of these local extremes are very shallow. Specifically, the difference between the value of this ratio at these two local extremes is about 4 %. For this reason, the authors are not certain if these two local extremes would appear if a different cross section set is used, due to the sensitivity of both Q_L and D_L to the energy dependence of the cross sections for elementary scattering processes.

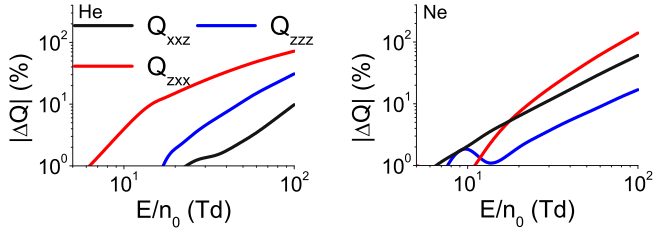

Fig. 10. The absolute value of the percentage difference between the two term and fully converged, multi term results, for the third-order transport coefficients of electrons in He and Ne.

(small values of t). In addition, this expression has been derived by using the Taylor expansion in terms of the components of the third-order transport tensor. For this reason, the expression (17) is applicable only when the ratios $Q_L/(t^{1/2}(D_L)^{3/2})$ and $Q_T/(t^{1/2}\sqrt{D_L}D_T)$ are not too large.

3.6 Comparison of the two term and fully converged multi term results

In Figure 10 we show the absolute value of the percentage difference between the two term and fully converged, multi term results, for the third-order transport coefficients of electrons in He and Ne. The absolute value of the percentage difference between the two sets of results for electrons in Ar, Kr and Xe is shown in Figure 11. The absolute value of the percentage difference ΔQ_{abc} is calculated as

$$|\Delta Q_{abc}| = \left|1 - \frac{Q_{abc}^{(TT)}}{Q_{abc}^{(MT)}}\right| \tag{34}$$

where the superscripts TT and MT refer to two term and multi term results, respectively.

We see that the two sets of results agree very well in the limit of the lowest E/n_0, where electrons undergo elastic collisions only. Specifically, the deviation between the results that are determined by these two methods is very low, up to approximately 8 Td, 17 Td, 0.2 Td, 0.35 Td, and 1.3 Td for electrons in He, Ne, Ar, Kr and Xe, respectively. The disagreement between these two methods for the off-diagonal components increases continuously with increasing E/n_0 until the end of the range of the considered E/n_0. Moreover, the deviation of multi term results for n^2Q_{xxz} and n^2Q_{zxx} from the corresponding two term results is much higher for electrons in Ar, Kr and Xe, as compared to the case of He and Ne. However, the behavior of the percentage difference between these two sets of results is somewhat different for the longitudinal component. While the disagreement between these two methods for the longitudinal component in He and Ne increases with increasing E/n_0, these methods, surprisingly, remain in a very good agreement for electrons in Ar, Kr and Xe, over the entire range of E/n_0 considered in this work. The percentage difference for the longitudinal component reaches values up to 30% and 17% for electrons in He and Ne, respectively, while it remains lower than 5% for electrons in Ar, Kr and Xe. We expect that the deviations between the two term and multi term results are much greater for the higher values of E/n_0. It should also be noted that the errors of the two term approximation are significantly lower for the lower-order transport coefficients, over the same region of E/n_0. Therefore, higher order transport coefficients appear more sensitive to anisotropy in the velocity distribution function.

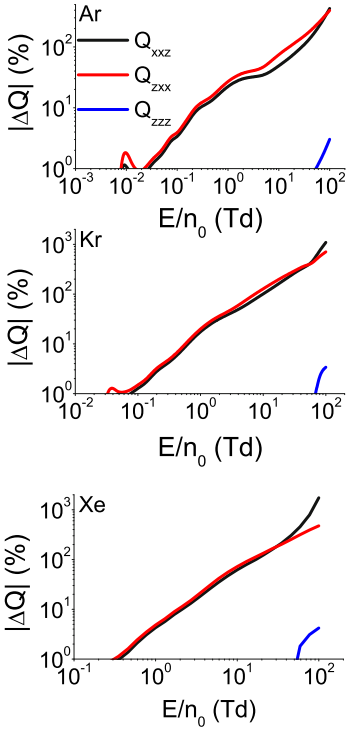

Fig. 11. The absolute value of the percentage difference between the two term and fully converged, multi term results, for the third-order transport coefficients of electrons in Ar, Kr and Xe.

4 Conclusion

In this work we have extended a multi term solution of the Boltzmann equation, initially developed for evaluating the lower-order transport coefficients, to investigate the third-order transport coefficients of electrons in noble gases. For electrons in helium, we have observed that the Q_{zxx} component is negative for the lower values of E/n_0. In this field region, the collision frequency for elastic scattering of a large fraction of electrons is an increasing function of the electron energy. However, for electrons in argon, krypton, and xenon all three components of the third-order transport tensor are positive in the limit of the lower fields considered in this work, as the collision frequency of the low-energy electrons decreases with increasing energy. For higher fields, the Q_{xxz} component is negative in argon, krypton and xenon over a wide range of E/n_0. In addition, for electrons in argon, the Q_{zxx} component is also negative, but over a narrower field range. For

electrons in helium in the sub-excitation field region, the absolute values of all three components of the third-order transport tensor are increasing functions of E/n_0. On the other hand, for electrons in argon, krypton and xenon, all components are significantly reduced over the range of E/n_0 where the energy of high-energy electrons exceeds the position of the Ramsauer-Townsend minimum.

One of the fundamental topics considered in this work is the existence of the correlation between the longitudinal component of the third-order transport tensor $n_0^2 Q_{zzz}$ and the longitudinal component of the diffusion tensor $n_0 D_{zz}$. We have observed that at high enough fields whenever $n_0 D_{zz}$ decreases or increases as a concave function of E/n_0 (in the log-log plot) $n_0^2 Q_{zzz}$ is being reduced. We have also observed that $n_0^2 Q_{zzz}$ increases when $n_0 D_{zz}$ increases as a convex function of E/n_0 (in the log-log plot). However, this correlation is absent in the limit of the lowest E/n_0, as the third-order transport coefficients vanish in the low-field limit, unlike diffusion which has non-zero thermal values. This behavior of $n_0^2 Q_{zzz}$ can be attributed to a greater sensitivity of the third-order transport coefficients with respect to the energy dependence of cross sections for elementary scattering processes.

Another highly relevant topic that has been investigated in this work is the influence of the third-order transport coefficients on the spatial profiles of the swarm in noble gases. It has been shown that this influence is the most pronounced for electrons in Ar, Kr and Xe, at low E/n_0, due to the presence of the Ramsauer-Townsend minimum. Specifically, the ratio $Q_L/(D_L)^{3/2}$ that describes the contribution of the longitudinal component of the third-order transport tensor to the spatial profile of the swarm reaches the first local maximum at about 10^{-3} Td, $7{\cdot}10^{-3}$ Td, and $1.9{\cdot}10^{-2}$ Td for electrons in Ar, Kr and Xe, respectively. Around these values of E/n_0 the effects of the longitudinal component of the third-order transport coefficient tensor on the spatial profile of the electron swarm are the most significant.

Finally, we investigated the deviation of the two term approximation from the fully converged multi term results for the third-order transport coefficients. We have found that the two term approximation is applicable at the lowest fields, where electrons undergo elastic collisions only. However, the two term approximation deviates from the multi term results for higher fields, where electrons may undergo inelastic collisions also with the background atoms. The difference between the two sets of results is especially pronounced for the off-diagonal components of the third-order transport tensor. This difference is much higher for electrons in Ar, Kr and Xe than for electrons in He and Ne. Conversely, the difference between the two sets of results for the longitudinal component is much larger in He and Ne than in Ar, Kr and Xe. This difference is up to about 30% and 17% for electrons in He and Ne, respectively. Surprisingly, the two term approximation is in an excellent agreement with the multi term results for the longitudinal component in the case of Ar, Kr and Xe. The difference between the results that are obtained by using these two methods is not higher than approximatelly 5% in the case of the longitudinal component of the third-order transport tensor for electrons in Ar, Kr and Xe.

This work was supported by the grants No. ON171037 and III41011 from the Ministry of Education, Science and Technological Development of the Republic of Serbia and also by the project 155 of the Serbian Academy of Sciences and Arts. RDW acknowledges the financial support of the Australian Research Council DP180101655.

Author contribution statement

All the authors have been involved in the research and in the preparation of the manuscript. All the authors have read and approved the final manuscript.

References

1. L.G.H. Huxley, R.W. Crompton, *The Diffusion and Drift of Electrons in Gases* (Wiley, London, 1974)
2. R. Robson, R. White, M. Hildebrandt, *Fundamentals of Charged Particle Transport in Gases and Condensed Matter* (CRC Press, Boca Raton, 2018)
3. Z.Lj. Petrović, M. Šuvakov, Ž. Nikitović, S. Dujko, O. Šašić, J. Jovanović, G. Malović, V. Stojanović, Plasma Sources Sci. Technol. **16**, S1 (2007)
4. S. Dujko, R.D. White, Z.Lj. Petrović, J. Phys. D: Appl. Phys. **41**, 245205 (2008)
5. Z. Donko, P. Hartman, I. Korolov, V. Jeges, D. Bošnjaković, S. Dujko, Plasma Sources Sci. Technol. **28**, 095007 (2019)
6. T. Makabe, Z.Lj. Petrović, *Plasma Electronics: Applications in Microelectronic Device Fabrication* (CRC Press, 2014)
7. M.A. Lieberman, A.J. Lichtenberg, *Principles of Plasma Discharges and Materials Processing*, 2nd edn. (Wiley, 2005)
8. D. Xiao, *Gas Discharge and Gas Insulation* (Springer, Heidelberg, 2016)
9. L. Rolandi, W. Riegler, W. Blum, *Particle Detection with Drift Chambers* (Springer, Berlin, 2008)
10. D. Bošnjaković, Z.Lj. Petrović, R.D. White, S. Dujko, J. Phys. D: Appl. Phys. **47**, 435203 (2014)
11. Z.Lj. Petrović, S. Dujko, D. Marić, G. Malović, Ž. Nikitović, O. Šašić, J. Jovanović, V. Stojanović, M. Radmilović Rađenović, J. Phys. D: Appl. Phys. **42**, 194002 (2009)
12. L.C. Pitchford et al., Plasma Process. Polym. **14**, 1600098 (2016)
13. A. Banković, S. Dujko, S. Marjanović, R.D. White, Z.Lj. Petrović, Eur. Phys. J. D **68**, 127 (2014)
14. A. Banković, S. Dujko, R.D. White, S.J. Buckman, Z.Lj. Petrović, Eur. Phys. J. D **66**, 174 (2012)
15. K. Kondo, H. Tagashira, J. Phys. D: Appl. Phys. **23**, 1175 (1990)
16. S. Kawaguchi, K. Takahashi, K. Satoh, Plasma Sources Sci. Technol. **27**, 085006 (2018)
17. B.M. Penetrante, J.N. Bardsley, in *Non-equilibrium Effects in Ion and Electron Transport*, edited by J.W. Gallagher, D.F. Hudson, E.E. Kunhardt, R.J. Van Brunt (Plenum, New York, 1990), p. 49

18. S.B. Vrhovac, Z.Lj. Petrović, L.A. Viehland, T.S. Santhanam, J. Chem. Phys. **110**, 2423 (1999)
19. J.H. Whealton, E.A. Mason, Ann. Phys. **84**, 8 (1974)
20. I. Simonović, D. Bošnjaković, Z.Lj. Petrović, P. Stokes, R.D. White, S. Dujko, Phys. Rev. E **101**, 023203 (2020)
21. A.D. Koutselos, J. Chem. Phys. **104**, 8442 (1996)
22. A.D. Koutselos, J. Chem. Phys. **106**, 7117 (1997)
23. A.D. Koutselos, Chem. Phys. **270**, 165 (2001)
24. A.D. Koutselos, Chem. Phys. **315**, 193 (2005)
25. H. Sugawara, Y. Sakai, Jpn. J. Appl. Phys. **45**, 5189 (2006)
26. Z.Lj. Petrović, I. Simonović, S. Marjanović, D. Bošnjaković, D. Marić, G. Malović, S. Dujko, Plasma Phys. Controlled Fusion **59**, 014026 (2017)
27. P.W. Stokes, I. Simonović, B. Philippa, D. Cocks, S. Dujko, R.D. White, Sci. Rep. **8**, 2226 (2018)
28. K. Kumar, H.R Skullerud, R.E. Robson, Aust. J. Phys. **33**, 343 (1980)
29. R.E. Robson, Aust. J. Phys. **44**, 685 (1991)
30. R.E. Robson, K.F. Ness, Phys. Rev. A **33**, 2068 (1986)
31. K.F. Ness, R.E. Robson, Phys. Rev. A **34**, 2185 (1986)
32. K. Kumar, Phys. Rep. **112**, 319 (1984)
33. R.D. White, R.E. Robson, S. Dujko, P. Nicoletopoulos, B. Li, J. Phys. D: Appl. Phys. **42**, 194001 (2009)
34. S. Dujko, R.D. White, Z.Lj. Petrović, R.E. Robson, Phys. Rev. E **81**, 046403 (2010)
35. S. Dujko, R.D. White, Z.Lj. Petrović, R.E. Robson, Plasma Sources Sci. Technol. **20**, 024013 (2011)
36. O. Šašić, J. Jovanović, Z.Lj. Petrović, J. de Urquijo, J.R. Castrejón-Pita, J.L. Hernández-Ávila, E. Basurto, Phys. Rev. E **71**, 046408 (2005)
37. R.D. White, R.E. Robson, P. Nicoletopoulos, S. Dujko, Eur. Phys. J. D **66**, 117 (2012)
38. M. Hayashi, *Bibliography of Electron and Photon Cross Sections With Atoms and Molecules Published in the 20th Century Argon Report, NIFS-DATA-72* (National Institute for Fusion Science of Japan, Tokyo, Japan, 2003)
39. M. Hayashi, *Bibliography of Electron and Photon Cross sections with Atoms and Molecules Published in the 20th Century Xenon, NIFS-DATA-79* (National Institute for Fusion Science of Japan, Tokyo, Japan, 2003)
40. Biagi-v7.1 database, www.lxcat.net (accessed 19 April 2013)